nature research

https://doi.org/10.1038/s41591-020-1039-5

Supplementary information

Dual CD4-based CAR T cells with distinct costimulatory domains mitigate HIV pathogenesis in vivo

In the format provided by the authors and unedited

Supplementary Figure 1.

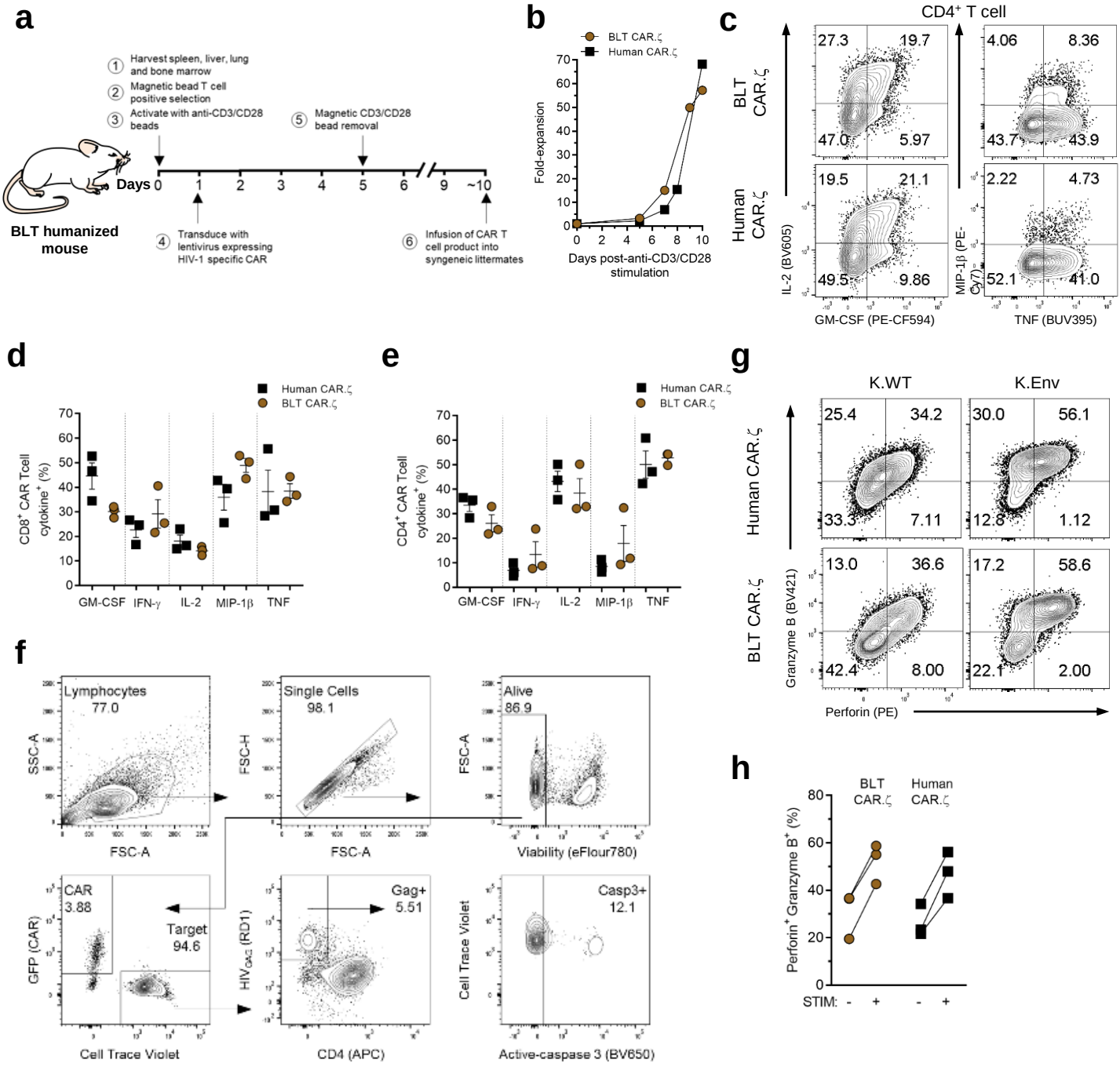

BLT-mouse derived HIV-specific CAR T cells are multifunctional *in vitro*. (a) Schematic for the manufacturing of BLT mouse-derived CAR T cells. **(b)** Representative growth kinetics of BLT mouse-derived and adult human PBMC-derived CAR.ζ T cells following activation with anti-CD3/CD28 Dynabeads. **(c)** FACS plots of CD4$^+$ CAR.ζ T cells expressing MIP-1β, TNF, IL-2 and GM-CSF after *in vitro* stimulation with HIV_{YU2} Envelope$^+$ K562 cells (K.Env). **(d)** Quantification of expression of the indicated intracellular protein by CD8$^+$ CAR.ζ T cells and **(e)** CD4$^+$ CAR.ζ T cells. Data shows expression of each protein from 3 biologically independent donors per source. **(f)** Schematic of gating strategy used to identify active caspase-3$^+$ HIV_{GAG}^+ target cells for analysis of HIV elimination assay. **(g)** FACS plots and **(h)** cumulative data demonstrating the coordinated upregulation of granzyme B and perforin in BLT mouse-derived and human donor-derived CAR.ζ T cells following *in vitro* stimulation with K.Env (+) or K.WT (-) cells. Data shows expression from 3 biologically independent donors per source. For data in **(d,e)**, line and error bars indicate mean ± SEM.

Supplementary Figure 2.

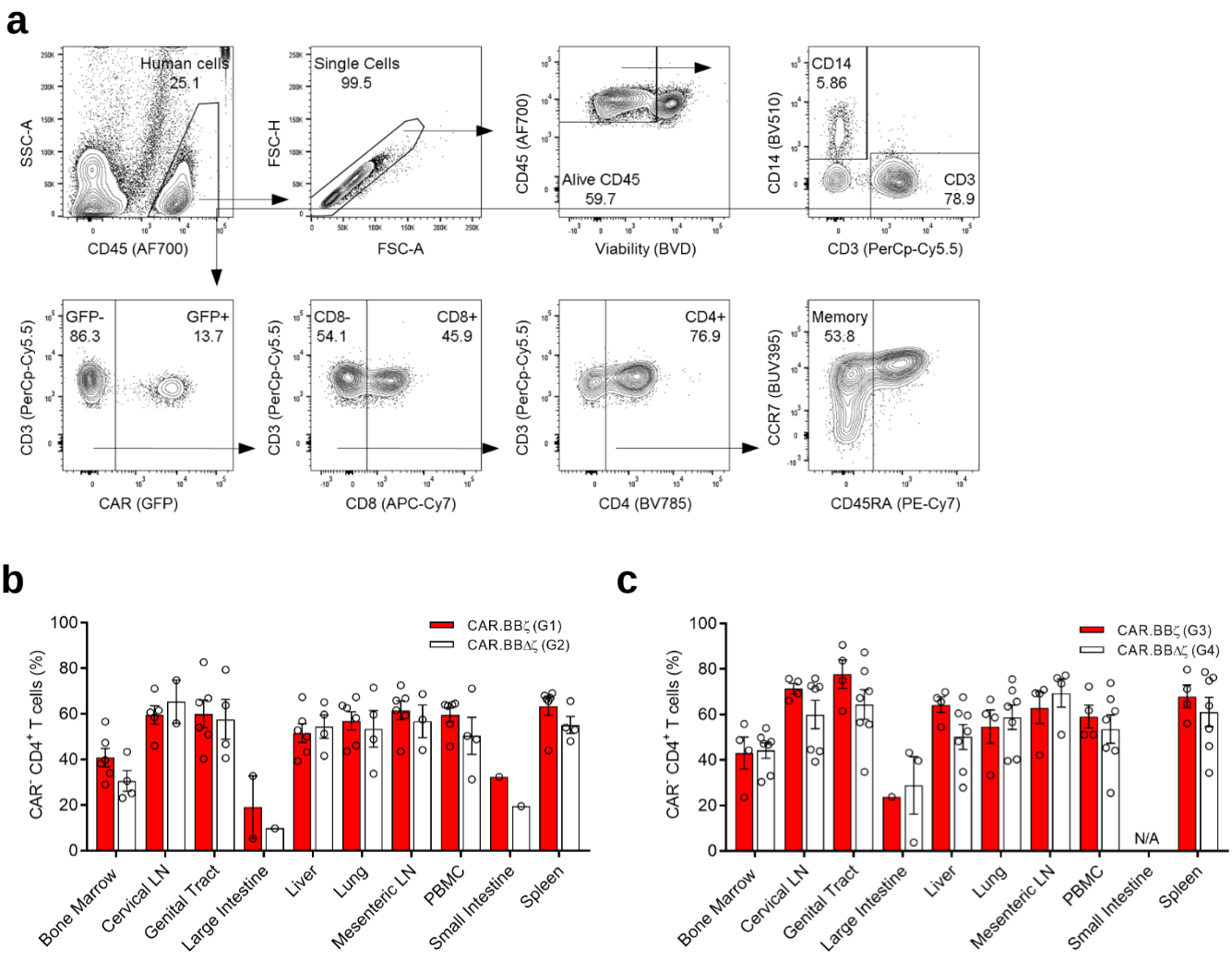

CAR.BBζ T cells fail to prevent CD4⁺ T cell loss after the discontinuation of ART. (a) Schematic of gating strategy used to identify total memory CD4⁺ T cells (CAR⁻). **(b)** Percentage of CD4⁺ T cells (CAR⁻) out of total CD3⁺ cells from the indicated tissues in BLT mice treated with CAR.BBζ T cells (G1; n=6) or control CAR.BBΔζ (G2; n=6) T cells, 12 weeks after the discontinuation of ART, and **(c)** 9 weeks after the discontinuation of ART for G3/4. Symbols represent biologically individual mice. Bars and error bars indicate mean ± SEM. N/A denotes tissue samples where viable human cells were too infrequent for analysis.

Supplementary Figure 3.

a

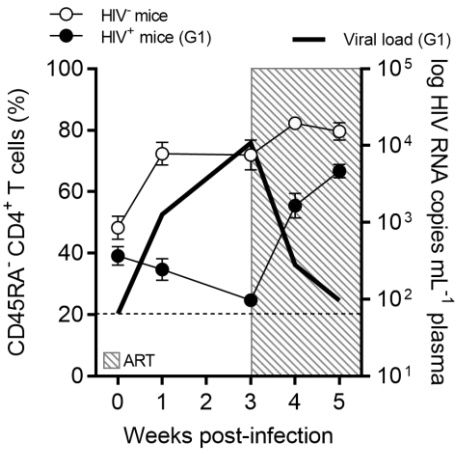

b

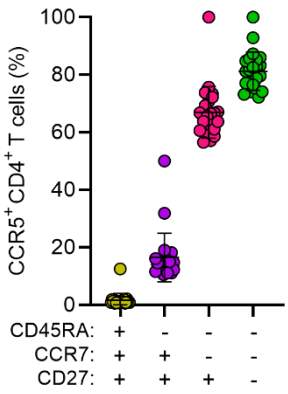

HIV infection preferentially depletes memory CD4⁺ T cells in BLT mice. (a) Mean plasma HIV RNA (copies mL^{-1}) for mice in G1 (n=6; thick line; right axis) and frequency of post-challenge peripheral memory ($CD45RA^-$) $CD4^+$ T cells in HIV^- mice (n=5; white circles) and HIV^+ mice (G1; black circles) (left y-axis). Thin dotted line denotes limit of viral load quantification. Shaded box indicates window of ART. Symbols and error bars indicate mean ± SEM. **(b)** Frequency of CCR5 expression on the indicated populations of $CD4^+$ T cells from the peripheral blood of BLT mice. Line and error bars represent mean ± SEM. Sample sizes in these studies represent biologically independent animals.

Supplementary Figure 4.

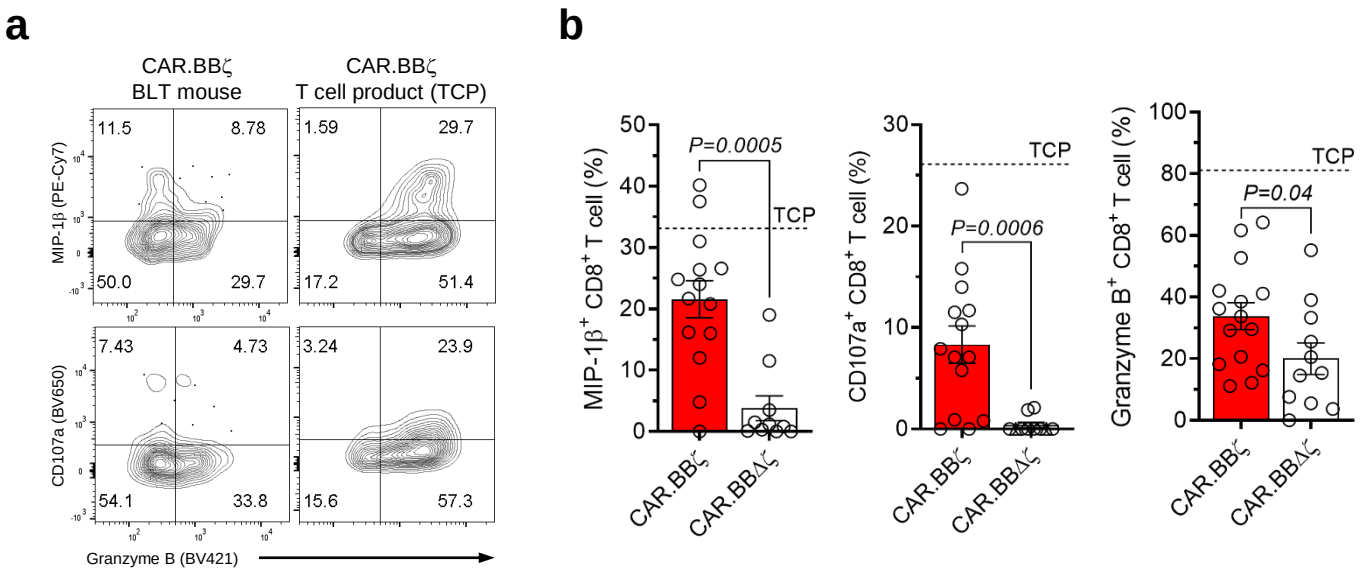

CAR.BBζ T cells from chronically infected mice exhibit attenuated *ex vivo* function compared to the pre-infusion CAR T cell product. CAR.BBζ T cells (n=14) and inactive control CAR.BBΔζ T cells (n=10) were isolated from the livers of chronically infected mice 12 weeks post-infusion, and the pre-infusion CAR.BBζ T cell product (TCP) were *ex vivo* stimulated with K.Env cells. **(a)** FACS plots and **(b)** cumulative data for the expression of MIP-1β, CD107a and granzyme B in $CD8^+$ CAR.BBζ or CAR.BBΔζ T cells. The dotted line indicates the frequency of $CD8^+$ CAR.BBζ T cells from the pre-infusion TCP expressing the indicated protein. Bars and error bars indicate mean ± SEM, and symbols represent individual mice. Significance was calculated using two-sided Wilcoxon rank-sum test. Sample sizes in these studies indicate biologically independent animals.

Supplementary Figure 5.

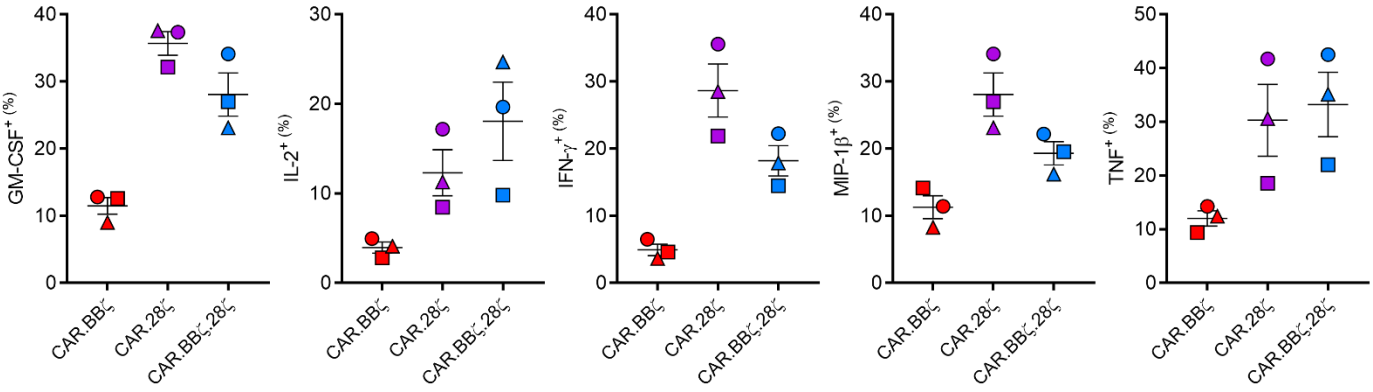

Dual-CAR T cells exhibit similar *in vitro* effector functions as CAR.28ζ T cells. The Dual-CAR T cell product comprises CAR.BBζ, CAR.28ζ, and Dual-CAR T cells, where each population is identified by a unique fluorescent protein. Upregulation of cytokines was measured after *in vitro* stimulation with K.Env and K.WT cells. Line and error bars show mean ± SEM. Data shows 3 biologically independent human donors where each symbol represents a different donor.

Supplementary Figure 6.

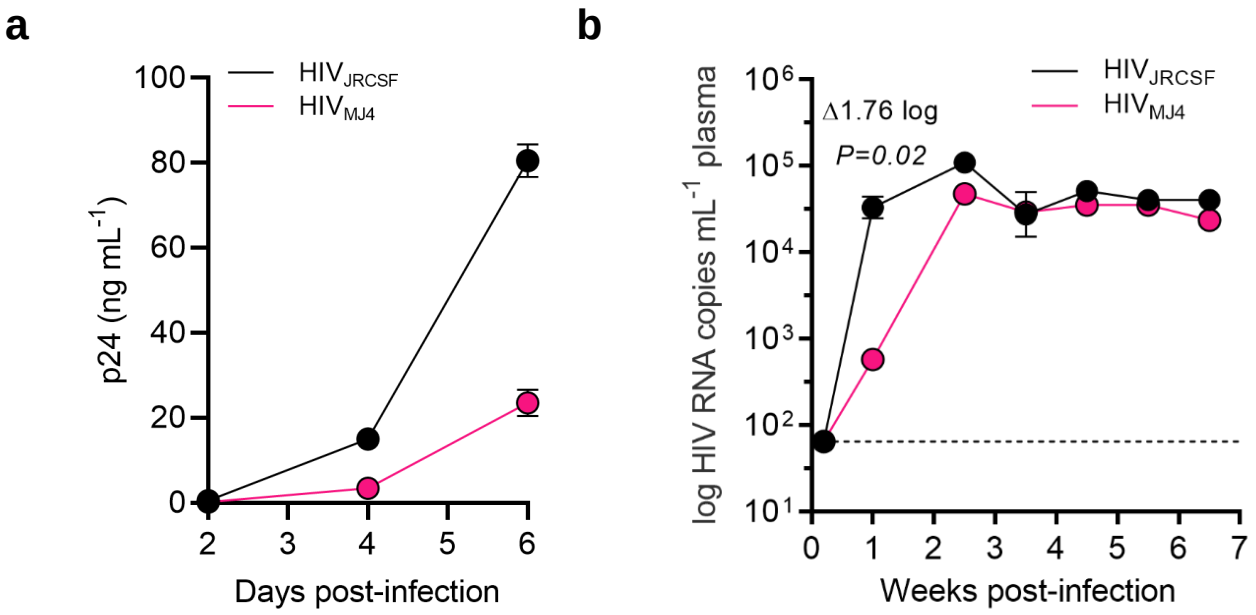

HIV$_{JRCSF}$ and HIV$_{MJ4}$ exhibit different replication kinetics *in vitro* and *in vivo*. (a) *In vitro* replication assay comparing the replication kinetics of HIV$_{JRCSF}$ and HIV$_{MJ4}$ in human PBMCs (n=3 technical replicates from a single human donor) stimulated with PHA and infected at a matched multiplicity of infection of 0.002. Virus replication was assessed by measuring p24 antigen in culture supernatants. **(b)** Mean log plasma HIV RNA (copies mL^{-1}) in BLT mice challenged with HIV$_{JRCSF}$ (n=3) or HIV$_{MJ4}$ (n=4). Thin dotted line denotes limit of quantification. Sample sizes indicate biologically independent animals. Significance was calculated using one-sided Wilcoxon rank-sum test. **(a,b)** Symbols and error bars indicate mean ± SEM.

Supplementary Figure 7.

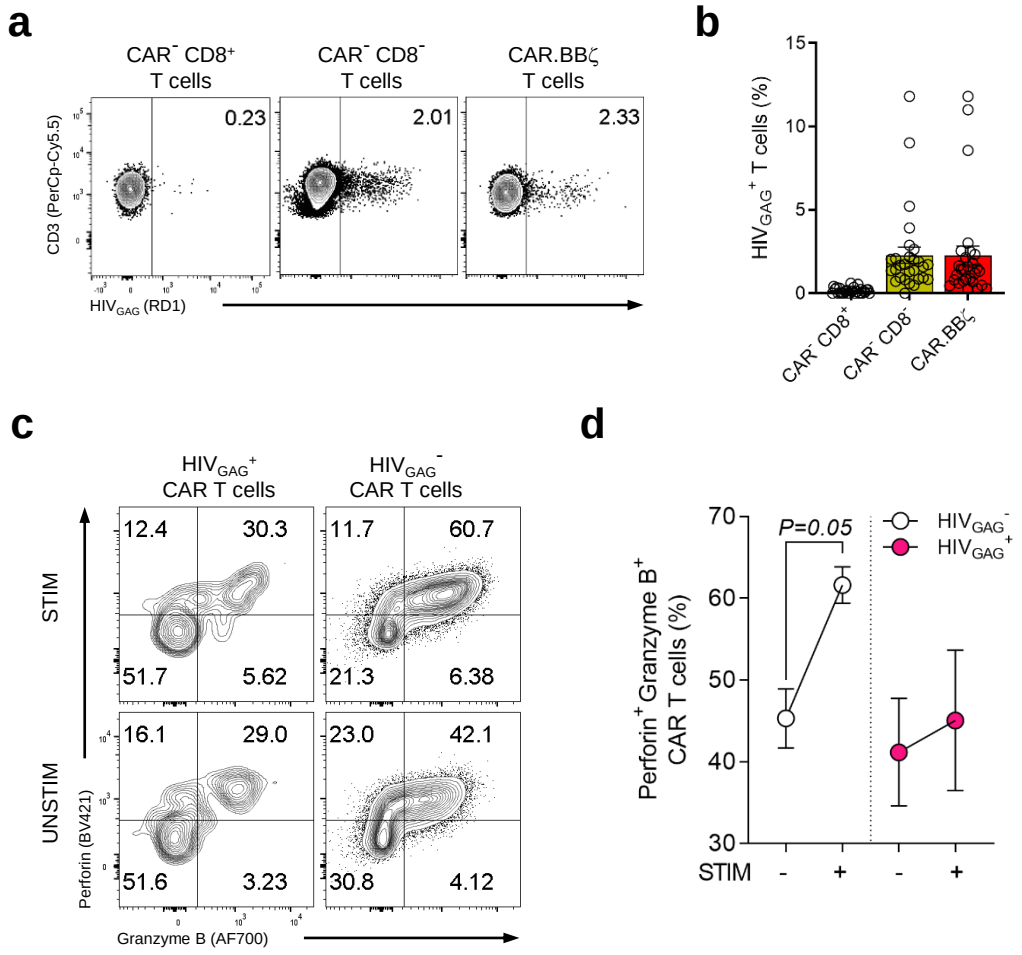

CD4-based CAR T cells are susceptible to infection *in vivo*. (a) FACS plots and **(b)** cumulative data show the frequency of HIV_{GAG}^{+} T cell populations sampled within the same mice (n=5) 10 weeks post-HIV_{JRCSF} infection. Data in **(b)** is the aggregate of tissues: bone marrow, liver, lung, lymph node, terminal blood, and spleen from 5 mice. **(c)** FACS plots and **(d)** cumulative data showing the expression of granzyme B and perforin within HIV_{GAG}^{+} and HIV_{GAG}^{-} CAR T cell populations from HIV_{JRCSF}-infected mice after *ex vivo* stimulation with K.Env (+) or K.WT (-) cells. For data in **(d)**, the data is represented as the average of 3 distinct CAR T cell populations isolated from one donor mouse. Significance was calculated using paired Student's t test. **(b,d)** Bars and symbols indicate mean and error bars show ± SEM.

Supplementary Figure 8.

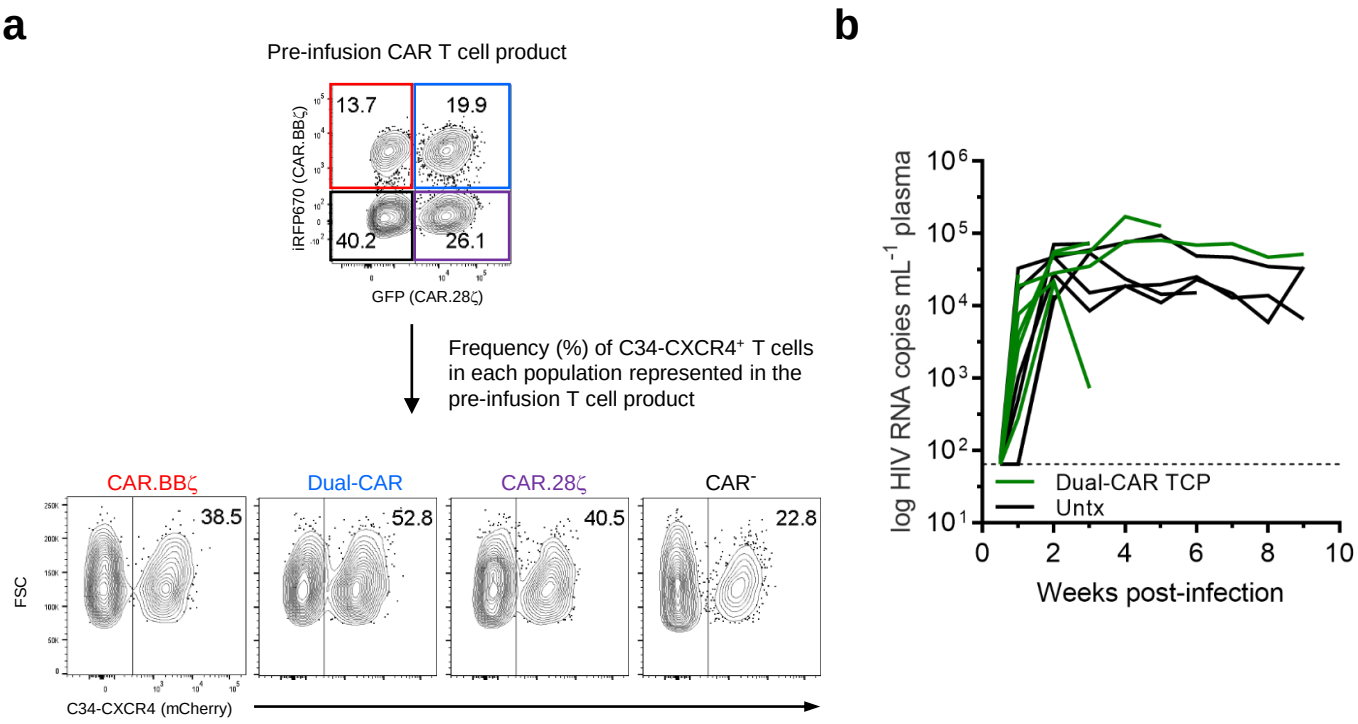

HIV-resistant Dual-CAR T cell product fails to inhibit acute HIV replication. (a) Dual-CAR T cell product (TCP) was co-transduced with C34-CXCR4 linked to mCherry by an intervening T2A sequence. FACS plots indicate the frequency of C34-CXCR4$^+$ cells within each cell population comprising the Dual-CAR TCP prior to infusion. **(b)** Log plasma viral RNA (copies mL^{-1}) in individual BLT mice challenged with HIV_{JRCSF} and 48 hours later mice were infused with HIV-resistant (C34-CXCR4$^+$) Dual-CAR TCP (n=7) or were untreated (Untx; n=7). Thin dotted line denotes limit of quantification. Sample sizes indicate biologically independent animals.

Supplementary Figure 9.

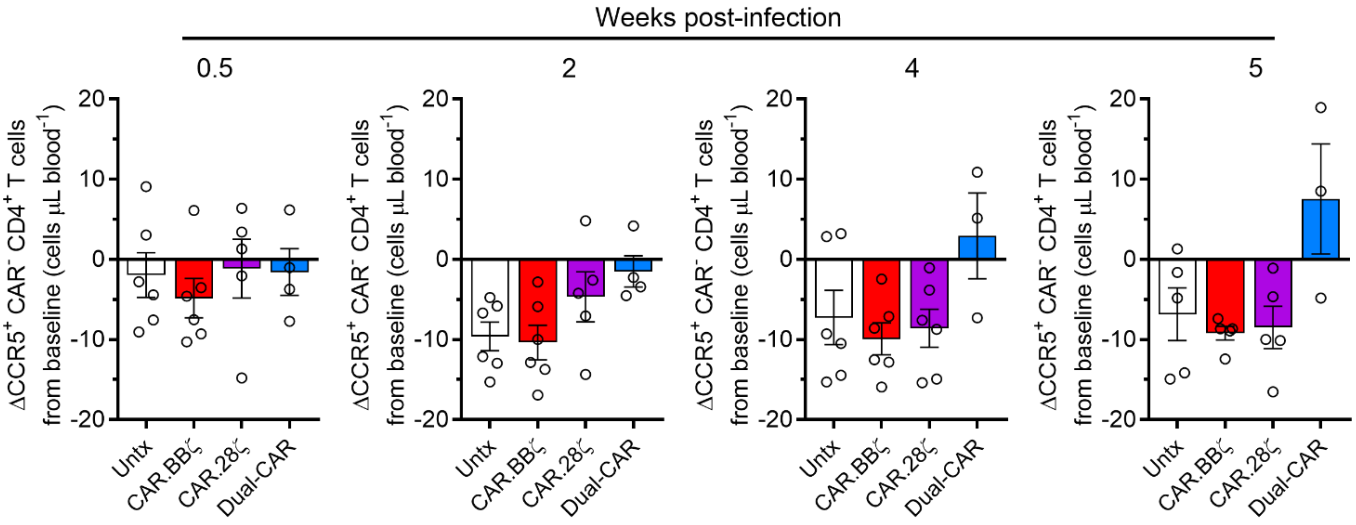

Low dose Dual-CAR T cells mitigate CD4⁺ T cell loss during HIV_{MJ4} infection. HIV_{MJ4}-infected mice were infused 48 hours post-challenge with 10^6 C34-CXCR4⁺, CAR.BBζ (n=6), CAR.28ζ (n=6), or purified Dual-CAR (n=4) T cells. For each group of mice, the change in peripheral cell concentration of CCR5⁺ CD4⁺ T cells (CAR^-) was measured from the indicated time post-infection to pre-infection levels. Bars indicate mean and error bars show ± SEM. Symbols represent biologically independent animals.

Supplementary Figure 10.

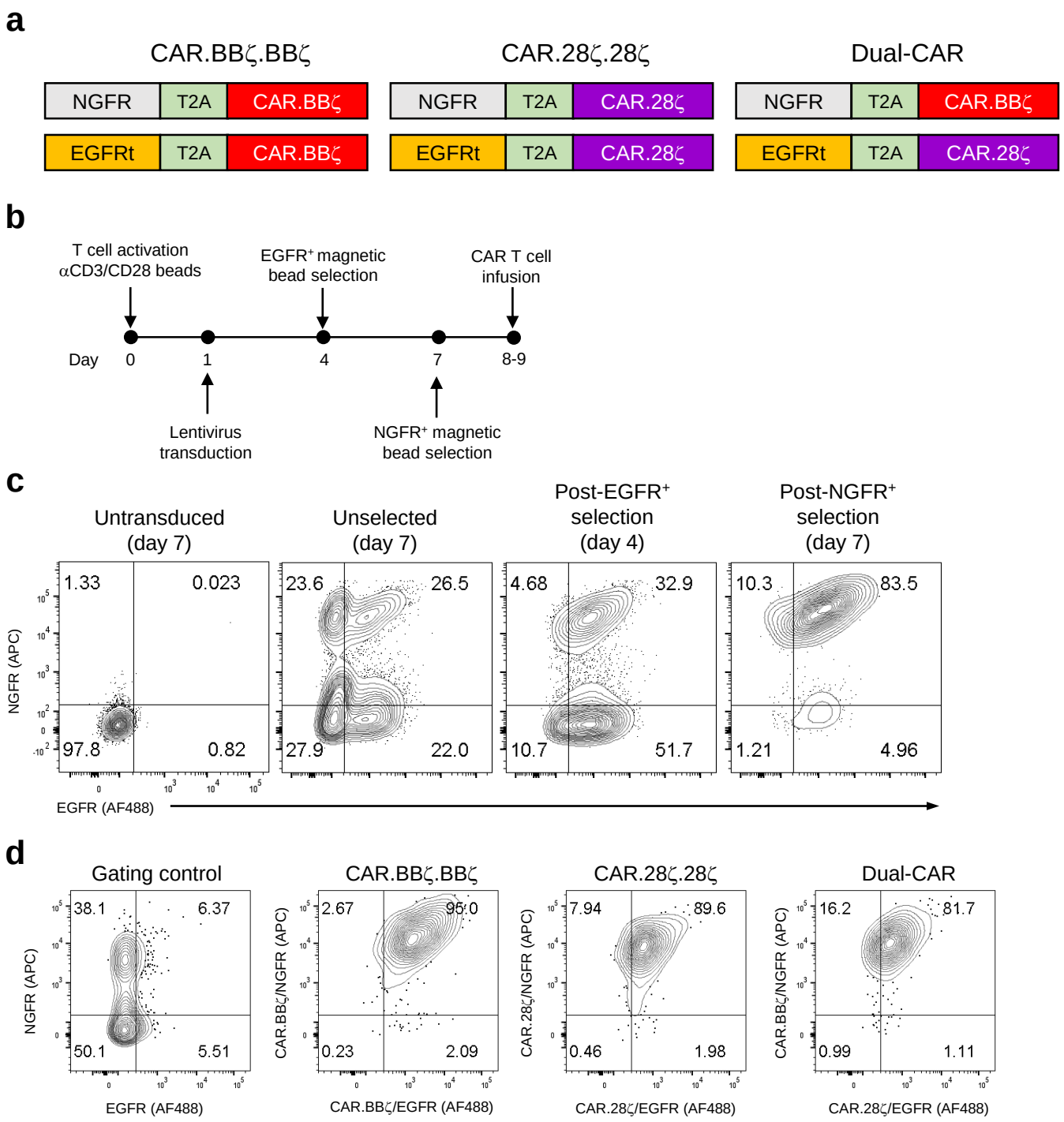

Two-step immunomagnetic selection process yields purified T cells expressing two independent CARs. (a) Schematic of lentivirus constructs used to generate dual CD4-based CAR T cells. The CD4-based CARs with the 4-1BB/CD3-ζ or CD28/CD3-ζ endodomains were linked with NGFR or truncated EGFR (EGFRt) to enable two-step positive magnetic selection during the T cell manufacturing process. **(b)** Time line for CAR T cell manufacturing. One day after T cell activation with αCD3/CD28 Dynabeads, the cells were transduced with an equivalent MOI of lentivirus depicted in **(a)**. On days 4 and 7 after activation, the CAR T cells were positively selected using anti-EGFR and anti-NGFR coated magnetic beads, respectively, as described in Materials and Methods. **(c)** Representative FACS plots illustrating the purity of CAR-transduced T cells after EGFR and NGFR selection. **(d)** FACS plots indicate the frequency of CAR.BBζ.BBζ, CAR.28ζ.28ζ, and Dual-CAR T cells post-selection in their respective pre-infusion T cell products, prior to adoptive transfer into mice described in **Figure 5e-n**.

Supplementary Figure 11.

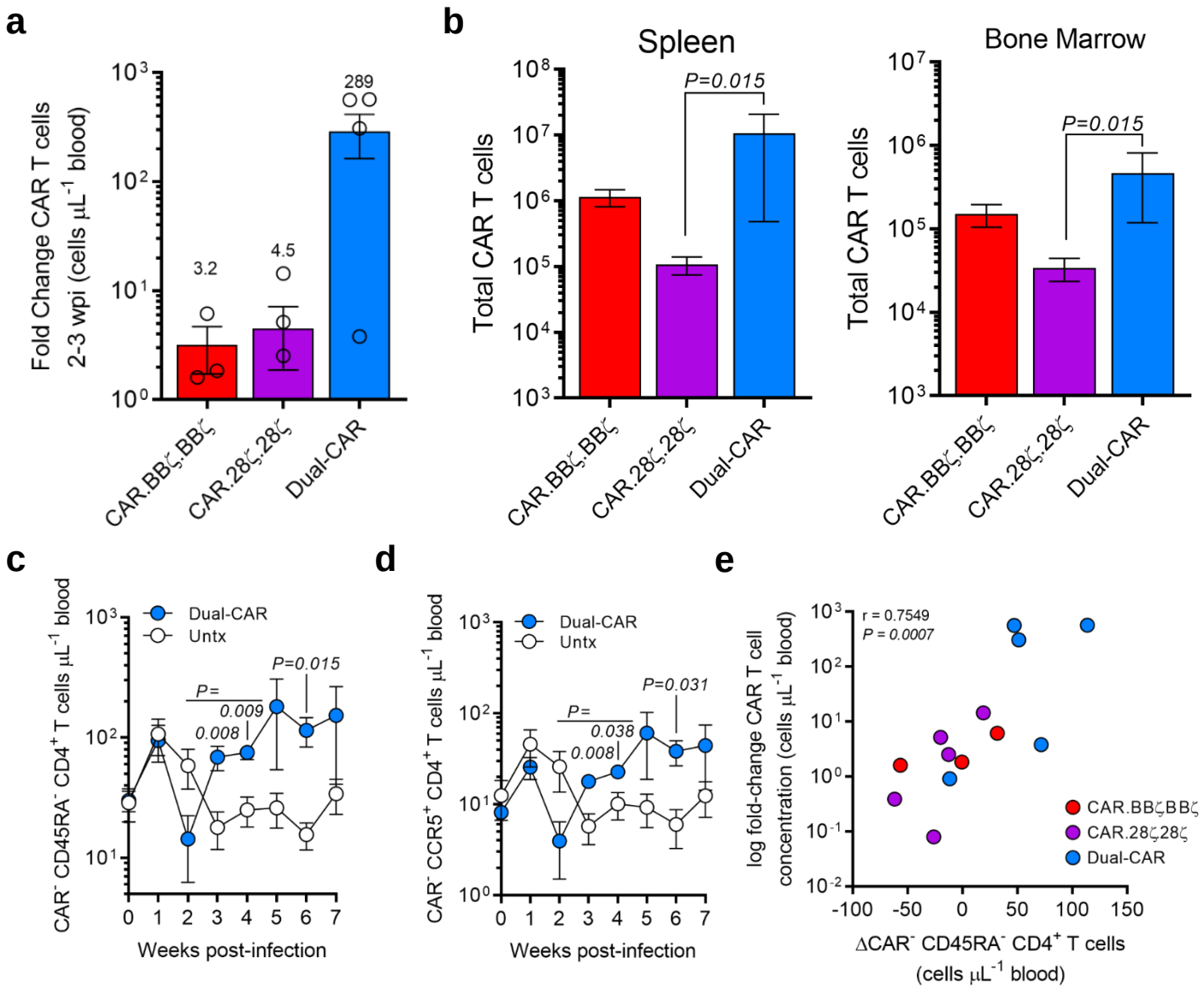

Dual-CAR T cells mediate superior expansion and protection of CD4⁺ T cells during HIV infection *in vivo*. BLT mice were infected with HIV_{MJ4} and 48 hours later received 10^6 C34-CXCR4⁺, purified CAR.BBζ.BBζ (n=5), CAR.28ζ.28ζ (n=5), Dual-CAR (n =5) T cells, or were untreated (Untx; n=4). **(a)** Fold-change in the concentration of CAR T cells in peripheral blood between weeks 2 and 3 post-infection. The number above the bars indicate mean fold-change. Symbols represent individual mice. Bars and error bars indicate mean ± SEM. **(b)** Absolute count of each CAR T cell population in tissues 8 weeks post-infection. **(c)** Concentration of peripheral total memory ($CD45RA^-$) and **(d)** $CD45RA^-$ $CCR5^+$ $CD4^+$ T cells (CAR^-). Symbols represent mean. **(e)** Association between fold-change in the concentration of CAR T cells and change in total memory ($CD45RA^-$) $CD4^+$ T cells (CAR^-) in peripheral blood between weeks 2 and 3 post-infection. Symbols represent individual mice. Spearman correlation test was used to calculate significance. **(b-d)** Error bars show ± SEM and two-sided Wilcoxon rank sum test was used to calculate significance. Sample sizes in these studies indicate biologically independent animals.

Supplementary Figure 12.

a

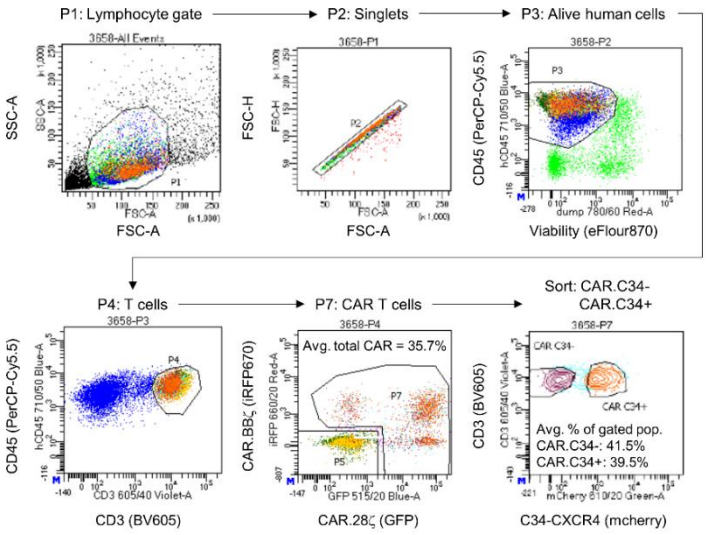

b

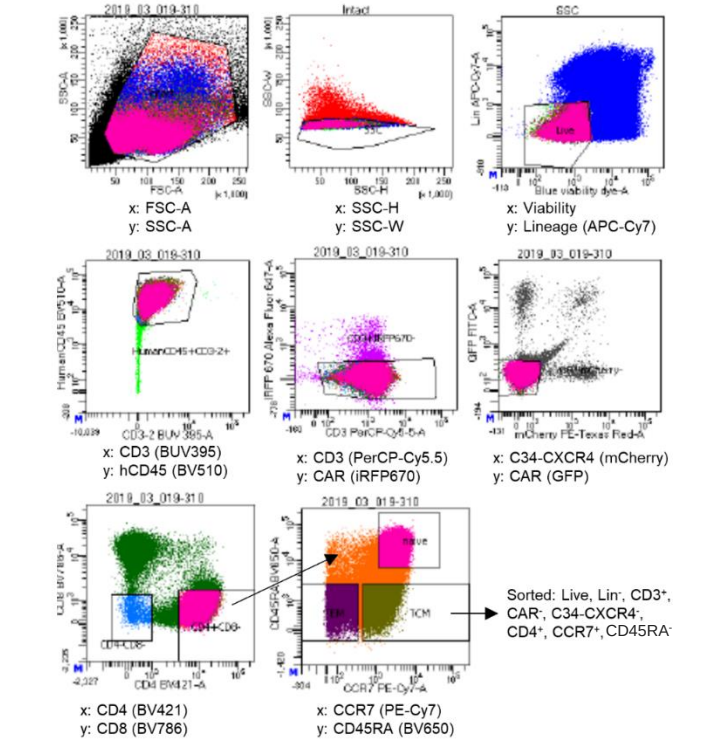

Gating strategy for FACS sorting of CAR T cells and endogenous central memory CD4⁺ T cells. (a) For the study described in **Figure 5b**, C34-CXCR4⁺ and C34-CXCR4⁻ CAR T cells were bulk sorted by FACS following the depicted gating strategy. **(b)** For the study described in **Figure 6e**, endogenous central memory CD4⁺ T cells (CAR⁻) were sorted from splenocytes harvested at necropsy (7 weeks post-infection) following the depicted gating strategy. For all data, cell-associated HIV DNA load was quantified on sorted cell populations by droplet-digital PCR.